Available online at www.sciencedirect.com

ScienceDirect

Advances in Space Research 67 (2021) 2643–2654

ADVANCES IN SPACE RESEARCH (a COSPAR publication)

www.elsevier.com/locate/asr

Durability characterization of mechanical interfaces in solar sail membrane structures

Jin Ho Kang [a,*], Keith L. Gordon [b], Robert G. Bryant [c], Olive R. Stohlman [d], W. Keats Wilkie [d], Amanda E. Stark [e], Randall S. Barfield [f], Benjamin R. Sindle [g], Miria M. Finckenor [h], Paul D. Craven [h]

[a] National Institute of Aerospace, Hampton, VA 23666, USA
[b] Advanced Materials and Processing Branch, NASA Langley Research Center, Hampton, VA 23681, USA
[c] Durability, Damage Tolerance and Reliability Branch, NASA Langley Research Center, Hampton, VA 23681, USA
[d] Structural Dynamics Branch, NASA Langley Research Center, Hampton, VA 23681, USA
[e] Structural and Thermal System Branch, NASA Langley Research Center, Hampton, VA 23681, USA
[f] NASA Langley Student Intern, University of Florida, Gainesville, FL 32611, USA
[g] NASA Langley Student Volunteer, Virginia Polytechnic Institute and State University, Blacksburg, VA 24061, USA
[h] Nonmetallic Materials and Space Environmental Effects Branch, NASA George C. Marshall Space Flight Center, Huntsville, AL 35812, USA

Received 6 March 2020; received in revised form 16 July 2020; accepted 9 August 2020
Available online 21 August 2020

Abstract

The construction of a solar sail from commercially available metallized film presents several challenges. The solar sail membrane is made by seaming together precut lengths of ultrathin metallized polymer film into the required geometry. This assembled sail membrane is then folded into a small stowage volume prior to launch. The sail membranes must have additional features for connecting to rigid structural elements (e.g., sail booms) and must be electrically grounded to the spacecraft bus to prevent charge build up. Space durability of the material and mechanical interfaces of the sail membrane assemblies will be critical for the success of any solar sail mission. In this study, interfaces of polymer/metal joints in a representative solar sail membrane assembly were tested to ensure that the adhesive interfaces and the fastening grommets could withstand the temperature range and expected loads required for mission success. Various adhesion methods, such as surface treatment, commercial adhesives, and fastening systems, were experimentally tested in order to determine the most suitable method of construction.
Published by Elsevier Ltd on behalf of COSPAR.

Keywords: Solar sail membrane; Polymer; Metal; Interface; Adhesion

1. Introduction

Solar sails are attractive spacecraft propulsion systems that offer extended mission capability by deriving thrust directly from momentum transfer of solar photons, rather than on-board propellant (Georgevic, 1973; McInnes, 1999; Tsu, 1959; Wilkie et al., 2011). The transferred photon momentum is very small but the acceleration can be maximized by increasing the surface area of the sail, and reducing the overall system mass. Since dimensions of commercially available metallized polymer membranes are limited, it is necessary to seam together preselected widths and thicknesses of a base material into the required sail membrane geometries. The assembled sail membranes must then be folded in a way suited for redeployment, and

* Corresponding author.
E-mail address: jin.h.kang@nasa.gov (J.H. Kang).

https://doi.org/10.1016/j.asr.2020.08.015
0273-1177/Published by Elsevier Ltd on behalf of COSPAR.

Nomenclature

λ	Wavelength (nm)
α	Absorptance (dimensionless quantity)
ε	Emittance (dimensionless quantity)
ρ	Reflectance (dimensionless quantity)
τ	Transmittance (dimensionless quantity)
LMW	Low molecular weight
PEN	Polyethylene naphtalate
PET	Polyethylene terephtalate
Al	Aluminum
Cr	Chromium
Be	Beryllium
HSEM	High-resolution scanning electron microscope
EDS	Energy dispersive X-ray spectrometry
MDSC	Modulated differential scanning calorimeter
TGA	Thermogravimetric analyzer

Subscripts

S	Solar
T	Thermal

stowed within a small volume prior to launch. Ensuring proper adhesion at the interfaces of the assembled sail film membranes throughout the entire mission lifecycle, including assembly, packaging, launch, deployment, and mission operations, is essential for overall mission success.

Silicone adhesive or pressure sensitive adhesive transfer tape has been widely used as a seaming method in space applications (Filsinger, 1995; Hanrahan and Ianno, 2014; White et al., 2010; Xiao et al., 2008). However, silicone adhesive requires a long period for cure, extra effort to produce uniform thickness and appropriate ventilation during application to prevent potential contamination of spaceflight hardware by uncured volatiles (Filsinger, 1995; White et al., 2010). In addition, silicone is degraded into low molecular weight (LMW) cyclic silicones by space radiation (Hanrahan and Ianno, 2014; Xiao et al., 2008), which can contaminate the reflective surface in the form of silicon oxides, resulting in reduced reflectivity.

The pressure sensitive adhesive transfer tapes are easy to apply. However, adhesive strength shows a large temperature dependency (50% decrease with a temperature increase of 70 °C) (3M, n.d.). The edge of the adhesive tape can damage the sail membrane during assembly, folding, and deployment if it inadvertently adheres to adjacent sail membrane areas.

Polyester-based hot-melt web adhesives have been widely used in textile industries because they are easy to apply, with a broad usage temperature, an absence of sticking issues after application, and good thickness control (Petire, 2013). Although they would be expected to improve fabrication efficiency of the sail, there has been no systematic study on adhesion durability of the polyester-based hot-melt adhesives for the solar sail application.

This study investigated the different interfaces of metal layer and polymer joints of sail structures including metal/-sail membrane (or metallized sail membrane) and metal/seaming adhesive joints. Optical and adhesion properties of a metallized sail membrane were characterized. A new seaming technology using the hot-melt web adhesive was demonstrated with the adhesion strength evaluated over a broad range of test temperatures to simulate the space environment.

2. Experimental

2.1. Materials

Metallized polyethylene naphthalate (PEN) films were used as a baseline representative solar sail membrane material. The core membrane material was purchased from Dupont Teijin (Teonex® Q72, 2 μm thick). The PEN core material was metallized via magnetron sputtering of aluminum (Al, 100 nm) on one side of the membrane (which serves as reflective layer) and chromium (Cr, 15 nm) on the opposite side (which serves as a thermal emittance layer for passive cooling). Metallization was performed by Astral Technology Unlimited, Inc. (MN, USA). Samples of Cr and Al at various thicknesses were also prepared for optical properties and mechanical adhesion testing. Metallization of these samples was performed via thermal evaporation (BOC Edwards auto 306 FL400 thin film deposition system).

Several additional metallized sail materials were also evaluated including aluminized polyethylene terephthalate (PET, Mylar®, Dupont, 2.54 μm), aluminized LaRC™ CP1 polyimide (CP1, 2.54 μm), and metallized polyimide (PI, Kapton® EN, 5 μm). Both aluminized PET and aluminized LaRC™ CP1 polyimide consisted of an Al layer (90 – 100 nm) deposited by e-beam evaporation. The metallized polyimide consisted of an Al (100 nm) layer on the front side of the membrane (the reflective layer) and Cr (30 nm) on the back side of the membrane (the thermal radiation layer). The aluminized PET material was purchased from SteinerFilm, Inc. (MA, USA). The aluminized LaRC™ CP1 polyimide (2.54 μm) was purchased from NeXolve Co. (AL, USA) and the metallized polyimide

(Kapton® EN, 5 μm) was obtained from Astral Technology Unlimited, Inc. (MN, USA).

Two polyester based hot-melt adhesives, PA 1811 (24 g/m^2, Spunfab Ltd., OH, USA) and PE 165 (14.5 g/m^2, Bostik Co., France) were evaluated for the solar sail seaming process.

2.2. Characterization

The thermo-optical properties [thermal emittance (ε_T), thermal reflectance (ρ_T), thermal transmittance (τ_T), solar absorptance (α_S), solar reflectance (ρ_S) and solar transmittance (τ_S)] were measured at room temperature using a portable emissometer (TEMP 2000, AZ Technology, AL, USA) in a wavelength rage of 3–30 μm with about ±1% accuracy and a laboratory portable spectroreflectometer (LPSR 300, AZ Technology, AL, USA) in a wavelength range of 250–2800 nm with about ±2% accuracy.

The adhesion strength of Al/PEN (or Al/Cr/PEN) joints was characterized by a peel resistance test (ASTM D1876) that measures the peel strength between two bonded flexible materials. This test is referred to a "T-peel test" because as the two adherends are pulled apart, they form the shape of a "T" as shown in Fig. 1. Plasma treatment was performed under air plasma for 30 min using XEI Scientific Evactron® Model 25. The radio frequency (RF) plasma power was measured at 20 J/s and the chamber pressure was 53 Pa. The thickness of the PEN membrane (2 μm) required an adhesive [poly(ethylene-co-methacrylic acid)] coated Al foil tape (~100 μm thick, Western Plastics, CA, USA) as backing material to create the sandwich structure, 10 mm wide and 90 mm long, shown in Fig. 1. A strip of Teflon™ film (~12 μm thick × 35 mm wide) was inserted between the PEN and adhesive layer to serve as a crack initiation point. This sandwich was placed in a hot press for about 7 min at 204 °C using a pressure range of 80–100 kPa to create the T-peel specimen.

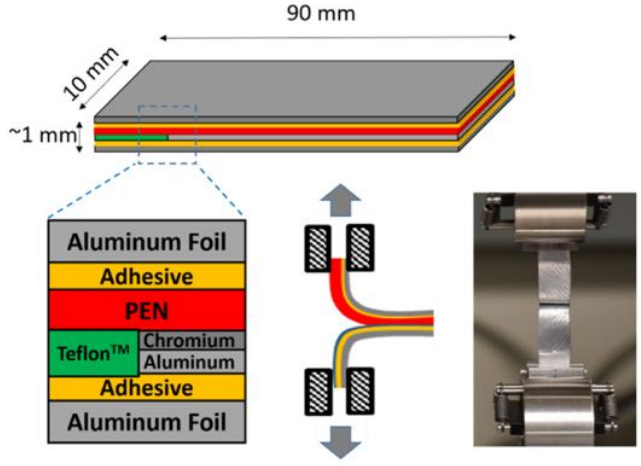

Fig. 1. Adhesion strength test specimen for metal/PEN joints (T-peel adhesion test, ASTM D1876).

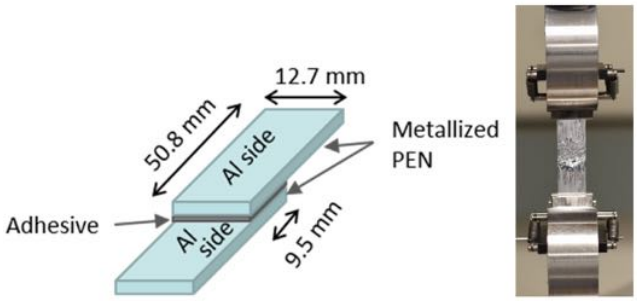

Fig. 2. Lap shear test specimen of the seamed solar sail membrane.

Adhesion strength of the seamed solar sail membrane joints using the hot-melt web adhesive was characterized according to a modified ASTM standard D5868. Due to the current sail membrane seaming design, the 12.7 mm × 9.5 mm overlap (adhesive size) was employed instead of the standard 25.4 mm × 25.4 mm overlap for the test. The hot-melt web adhesive was placed between the Al side of sail membrane and Cr side of sail membrane. The test specimen and test fixture are shown in Fig. 2. At least five tests were taken to get a statistical average.

A Hitachi S-5000 high-resolution scanning electron microscope (HSEM), equipped with a field emission electron gun and in-lens detector, was used to examine the surface morphology of the metallized PEN film. The locus of failure was evaluated by element analysis using energy dispersive X-ray spectrometry (EDS, EDAX Inc., NJ, USA).

The thermal properties of melting, crystalline and glass transition temperature of the metallized PEN film were characterized at a heating rate of 3 °C/min and thermally cycled at ±0.47 °C/min using a modulated differential scanning calorimeter (MDSC, Q20, TA Instruments, DE, USA). Thermo-oxidative stability of the hot-melt adhesives was characterized at a heating rate of 10 °C/min in air using a thermogravimetric analyzer (TGA, Q50, TA Instruments, DE, USA).

3. Results and discussion

3.1. Candidate sail materials for NASA solar sails

Membrane structures and optical properties of the candidate solar sail materials are summarized in Tables 1–3. Kapton® EN polyimide, was selected as a sail membrane for the Sunjammer project (Heiligers et al., 2014). It has relevant thermal and mechanical properties and is an excellent candidate material for the harsh space environment. The film has a reflective Al layer (100 nm, $\rho_S \sim 0.9$) on the front side, and Cr (30 nm, $\varepsilon_T \sim 0.48$) on the back side for passive cooling. However, an ultrathin film (less than 5 μm) is not commercially available due to manufacturing limitations. Compared to Kapton® EN polyimide, LaRC™ CP1 polyimide (colorless polyimide) has less yellow or tan color, due to charge transfer between the fluorinated poly-

Table 1
Candidate sail membrane materials for recent NASA solar sail projects.

Material ID	Sail Structure (material/thickness)			Comment
	Reflective Coating	Core Polymer	Emissive Coating	
Metallized PI	Al/100 nm	Kapton® EN/5 μm	Cr/30 nm	Sunjammer
Aluminized CP1	Al/90 nm	LaRC™ CP1/2.54 μm	No coating	NEA Scout
Aluminized PET	Al/100 nm	PET/2.54 μm	No coating	ACS3
Metallized PEN	Al/100 nm	PEN/2 μm	Cr/15 nm	ACS3

Table 2
Solar optical properties of candidate sail membranes (λ_s: 250–2800 nm).

Material ID	Side	α_S	ρ_S	τ_S
Metallized PI	Al	0.10	0.90	0.00
	Cr	0.54	0.46	0.00
Aluminized CP1	Al	0.10	0.90	0.00
	CP1	0.17	0.83	0.00
Aluminized PET	Al	0.09	0.91	0.00
	PET	0.14	0.86	0.00
Metallized PEN	Al	0.10	0.90	0.00
	Cr	0.57	0.43	0.00

Table 3
Thermal infrared properties of candidate sail membranes (λ_T: 3–30 μm).

Material ID	Side	ε_T	ρ_T	τ_T
Metallized PI	Al	0.03	0.97	0.00
	Cr	0.48	0.52	0.00
Aluminized CP1	Al	0.03	0.97	0.00
	CP1	0.29	0.71	0.00
Aluminized PET	Al	0.02	0.98	0.00
	PET	0.25	0.75	0.00
Metallized PEN	Al	0.03	0.97	0.00
	Cr	0.60	0.40	0.00

mer backbones. The solubility of LaRC™ CP1 polyimide allows for membrane fabrication as thin as 2.54 μm via solution casting. Unfortunately, the high cost of the LaRC™ CP1 polyimide is a major obstacle in expanding its applications. The aluminized LaRC™ CP1 is considered for use for the Near-Earth Asteroid (NEA) Scout project. These aluminized PET or metallized PEN films are candidate sail membranes for the NASA Advanced Composite Solar Sail System (ACS3) project (Wilkie et al, 2019) as their physical and thermal properties are suitable for this mission.

3.2. The effect of Cr layer thickness on optical properties of sail membranes

The equilibrium temperature of a solar sail membrane exposed to sunlight in space is, to the first order, determined by the α_S and ε_T of the membrane surfaces. The ε_T of the non-Sun facing side has the largest effect on the temperature of the sail by thermal radiation (passive cooling).

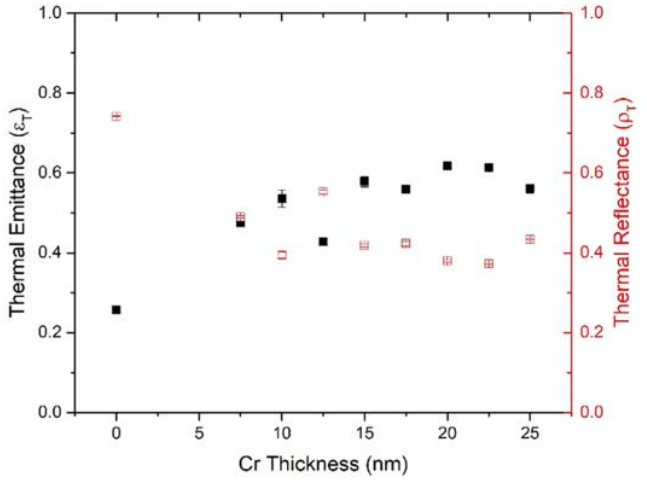

Fig. 3. The effect of Cr thickness on ε_T and ρ_T of Cr side of the Al (100 nm)/PET (2.54 μm)/Cr sail membrane.

Thus, it is important to examine the effect of the Cr coating thickness on the ε_T. Cr layers with different thickness (7.5 ~ 25 nm) were deposited on the aluminized PET membrane samples (Table 1) by thermal evaporation. The thickness of the Al layer for the Sun-facing side was fixed at 100 nm for solar radiation reflection (Kang et al., 2017) and this also met the minimum requirement for maximum solar radiation reflection (Kezerashvili, 2008, 2009).

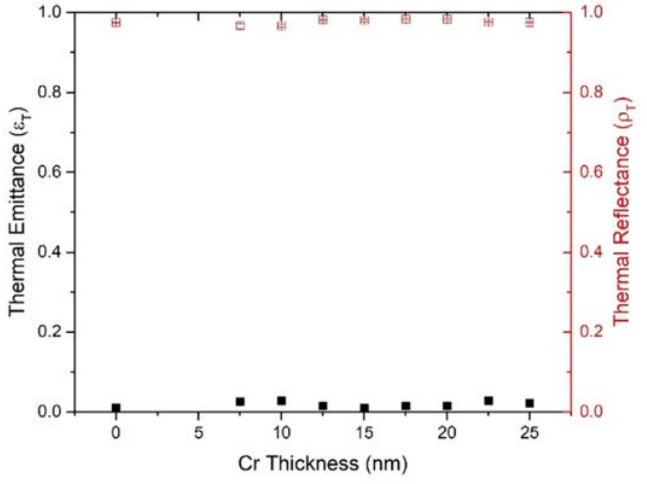

Fig. 4. The ε_T and ρ_T of the Al side of the Al (100 nm)/PET (2.54 μm)/Cr sail membrane.

Fig. 3 shows the ε_T and ρ_T of the Cr side as a function of the Cr thickness. The ε_T of the PET side (no Cr) was 0.26, and increased with increasing Cr coating thickness, 0.47 for 7.5 nm thick Cr, and 0.62 for 20 nm thick Cr. Over 20 nm in thickness, the ε_T of Cr side did not exhibit further increase and slightly decreased at 25 nm thickness. The ε_T of 12.5 nm thick Cr showed an unexpected drop from the trend, and a further investigation is ongoing. The ε_T of Cr side showed a trend opposite that of the ε_T of Cr as the transmittance was near zero.

The ε_T (~0.02) and ρ_T (~0.98) of the Al side did not change with the thickness of the Cr layer. This is because the Al layer, at 100 nm, is completely opaque, and the optical properties of the Al side are not affected by the Cr surface on the opposite side (Fig. 4).

The effect of the Cr thickness on the optical properties of the metallized PEN sail membrane was investigated (Fig. 5). Different thicknesses of Cr and Al were deposited on the raw PEN membrane by thermal evaporation. The trend was similar to the metallized PET sail membrane. The ε_T of the PEN side (no Cr) was 0.28, and it increased with increasing Cr thickness ($\varepsilon_T \sim 0.51$ for 7.5 nm thick Cr and $\varepsilon_T \sim 0.67$ for 20 nm thick Cr). Over 20 nm in thickness, the ε_T of Cr showed a slight decrease (for 25 nm thick Cr, $\varepsilon_T \sim 0.61$).

The ε_T (~0.04) and ρ_T (~0.96) of the Al layer did not change with the different Cr layer because of near zero transmittance through the thick Al layer (Fig. 6).

3.3. Thermal analysis of sail membranes in low Earth orbit

PEN shows slightly higher thermal and mechanical durability than PET, has the requisite mission-enabling properties, and has a similar price point. Thus, the PEN membrane was selected for the further study (MacDonald et al., 2007). Thermal environmental analysis of the baseline ACS3 metallized PEN membrane (Al/PEN/Cr) was

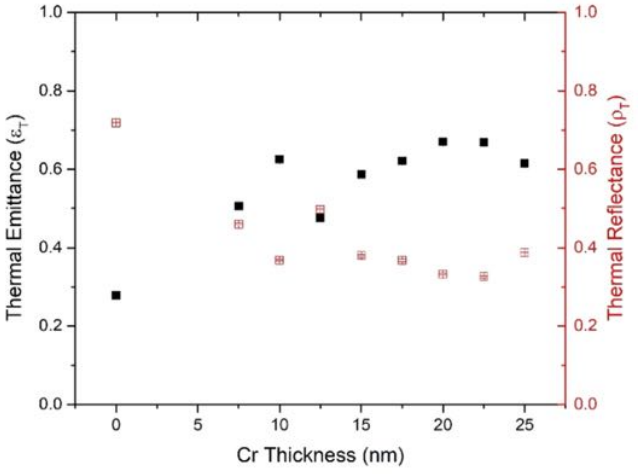

Fig. 5. The effect of Cr thickness on ε_T and ρ_T of Cr side of the Al (100 nm)/PEN (2 μm)/Cr sail membrane.

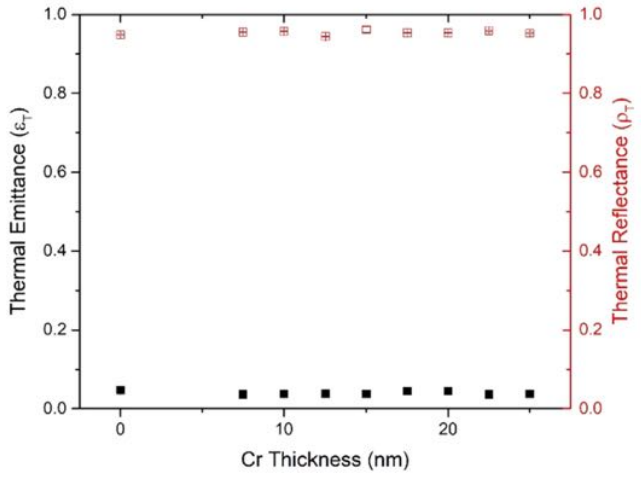

Fig. 6. The ε_T and ρ_T of Al side of the Al (100 nm)/PEN (2 μm)/Cr sail membrane.

calculated using Thermal Desktop 6.0 Patch 21. The sail was simulated by starting with an Autodesk drawing of the shape of the sail and then generating a finite element method (FEM) mesh of the surface. Next, thermophysical and optical properties were added. The thermophysical properties for PEN were used. The optical properties were collected directly from the corresponding side of the sail membrane (Tables 2 and 3 in section 3.1.). The analysis used a polar orbit with an inclination of 98°, the right ascension of the ascending node (RAAN) of 270°, and an altitude of 700 km. Fig. 7 shows the Thermal Desktop visual representation of the polar orbit used in this study.

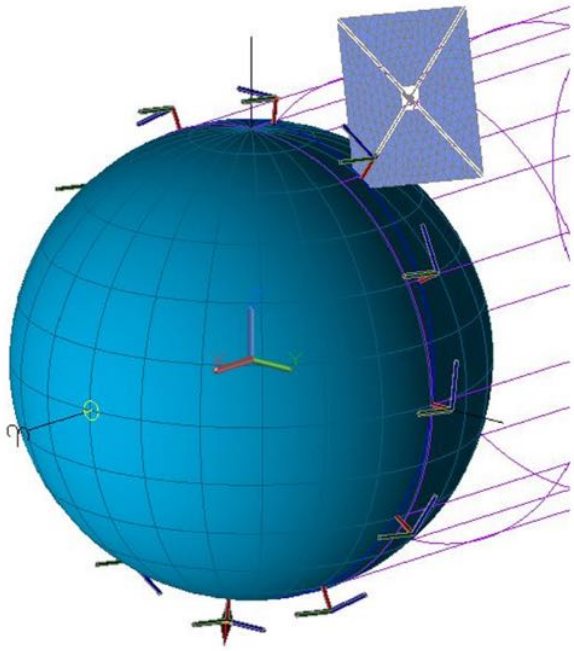

Fig. 7. Reference 700 km, 98° inclination dawn-dusk Sun-synchronous polar orbit for sail thermal equilibrium analyses. The sail surface normal is perpendicular to the orbit plane. Sail is not to scale.

During a loss of attitude control, the sail may begin to tumble and experience arbitrary orientations with respect to the Sun while attitude control is being re-established. Thermal analyses of on-orbit sail temperatures need to include cases where the orientation is not optimal. This resulted in four orientation cases; (i) correct orientation with Al coating facing Sun, (ii) reversed orientation with the Cr coating facing the Sun, (iii) edge to the Sun with the Al coating point nadir, and (iv) edge to the Sun with the Cr coating pointing nadir. All cases calculated temperatures of the sail quadrants over the course of one complete orbit. Thermal Desktop has a tool that determines the maximum and minimum temperature for a specific part of the model. This tool simplified identifying the maximum and minimum temperature of all four sail quadrants, with the results shown in Table 4. These temperatures were selected for determining the sail membrane adhesion testing thermal conditions in the following sections.

Beryllium (Be) has been studied for space mirror and sail membranes because of its lower density, higher Young's modulus and higher strength compared to Al (Kezerashvili and Matloff, 2007; Matloff and Kezerashvili, 2008). The thermal environmental analysis of a Be coated sail membrane as an alternative was calculated as shown in Table 5. Solar absorptance and thermal emittance of Be were chosen as 0.33 and 0.25 for this calculation (Gauthier et al., 2015; Loarer et al., 2007). The Be coated sail membrane showed higher a thermal equilibrium temperatures of 62.8–67.2 °C with the Be surface towards the Sun and lower temperature with its Cr surface towards the Sun (98.5–103.1 °C) compared to the Al coated sail membrane. Due to contamination issues associated with the Be coating process, it is not considered as a reflective layer for the current NASA sail missions.

3.4. Sail membrane interfaces

The baseline ACS3 solar sail membrane quadrant was assembled from 75 cm wide metallized PEN membrane strips or gores. Thirteen PEN membrane gores were seamed together to form a sail quadrant with a 9.2 m edge. Fig. 8 shows two quadrant sail membranes fabricated by seaming metallized sail membrane material. There are several interfaces in the sail membrane: Al/PEN, PEN/Cr, Cr/adhesive and adhesive/Al. In Sections 3.5 and 3.6, each interface is outlined.

3.5. The interfaces of between metal layers and sail core membranes

For the baseline Al/PEN/Cr sail material, there are two metal-to-polymer interfaces: the Al/PEN and Cr/PEN interfaces. Compared to Cr/PEN, Al/PEN has weaker interfacial strength (Silvain and Ehrhardt, 1993; Cordill et al., 2010) and local delamination of the Al layer was observed from creasing and wear during fold/stowage. The delamination of the Al layer increased with moisture in the laboratory atmosphere. Thus, the adhesion strength was investigated using a T-peel adhesion test (ASTM D1876, Fig. 1) and several adhesion promotion methods were tested.

The adhesion strength of the baseline Al/PEN joint was 202.9 N/m (Fig. 9). Plasma treatment (20 J/s, 30 min, 53 Pa) of the PEN film before deposition of the Al layer improved the adhesion strength by 17% (238.4 N/m). The stronger interfacial strength seems to originate from the cleaning effect due to the increased surface energy that can be attributed to polar components such as hydroxyl groups (Liston et al., 1993). Thus, the plasma treatment was employed as a pre-treatment process for further tests. When a Cr layer was deposited on the plasma treated PEN as a tie-layer prior to Al layer deposition, further improvement of 41–76% (286.6–357.1 N/m) was achieved for 2.5 –10 nm thick Cr tie layers. The Cr tie layer of 7.5 nm thickness showed the highest adhesion strength (357.1 N/m). However, the PEN membranes ruptured during the test (cohesive failure in adherend). The actual adhesion strength, or interfacial strength, between Al-Cr and the PEN could be higher than the measured values as shown by the arrows on the data columns (Kang et al., 2001). This result suggests that the plasma treatment and Cr tie layer (about 7.5 nm thick) can be a viable way to increase the adhesion strength of metallized PEN joints.

3.6. The interfaces of metallized PEN membranes seaming joints

As previously mentioned, the use of pressure sensitive adhesive creates a sticking issue. To mitigate this problem, a hot-melt adhesive was selected as an alternative. Table 6 shows two candidate unwoven matted polyester fiber web hot-melt adhesives. While PA1811 has a melting point of 75 °C, PE 165 has a higher melting point of 165 °C and

Table 4
The maximum and minimum temperature that the Al coated sails (Al/PEN/Cr) experience for each orientation.

Orientation	Temperatures (°C)	
	Max	Min
Al surface toward Sun	4.6	0.1
Cr surface toward Sun	136.5	131.0
Sail edge toward Sun, Al surface toward nadir	16.4	−27.0
Sail edge toward Sun, Al surface toward zenith	−16.6	−126.3

Table 5
The maximum and minimum temperature that the Be coated sails (Be/PEN/Cr) experience for each orientation.

Orientation	Temperatures (°C)	
	Max	Min
Be surface toward Sun	67.2	62.8
Cr surface toward Sun	98.5	103.1
Sail edge toward Sun, Be surface toward nadir	−77.3	−10.7
Sail edge toward Sun, Be surface toward zenith	−47.4	−4.3

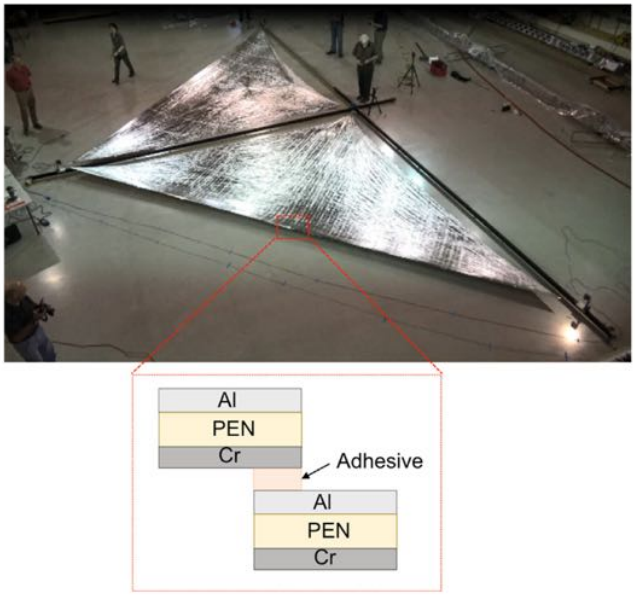

Fig. 8. Sail quadrant deployment test. The cross-sectional structure of the seamed sail membranes is shown in an inset. The edge of sail is 9.2 m.

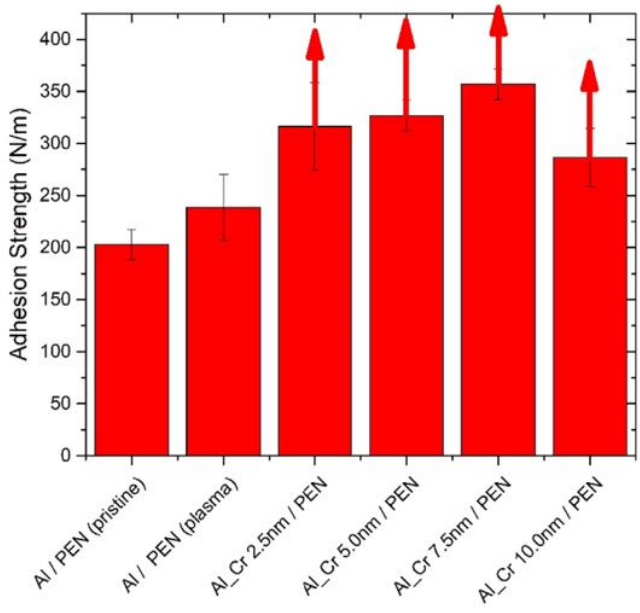

Fig. 9. Adhesion strength of Al/PEN and Al-Cr/PEN joints. Arrows indicate that the actual adhesion strength could be higher than the measured adhesion strength because cohesive failure in adherend (sail membrane) occurred.

was selected for the seaming test in this study. The optimum condition (at least 180 °C) for the hot melt process was estimated from the 1st heating run of the MDSC thermogram, and the maximum operation temperature for long-term application was suggested from the onset point (140 °C) of the melting peak of the 2nd heating run (Fig. 10). Also, PE 165 has low water absorption and exhibited good thermo-oxidative stability at the seaming condition (180 °C), and 5% weight loss at 330 °C at a heating rate of 10 °C/min (Fig. 11). Further investigation of isothermal stability is required.

Fig. 12 shows the seaming process. The PE 165 adhesive was cut into strips of ~9.5 mm and placed on the Cr side of the metallized PEN membrane gore. The adhesive was covered by another metallized PEN gore with the Al side down and fused with a temperature controlled iron. PEN can shrink at high temperature (0.2% at 200 °C) (MacDonald et al., 2007), but noticeable shrinkage was not observed.

The seamed-joint adhesive strength was evaluated by a modified ASTM standard D5868 lap shear test to simulate tensile loading of the adhesive joints of the deployed solar sail membrane. The test specimen and test fixture are shown in Fig. 2. Visual failures of adhesion test specimens are shown in Figs. 13 and 19. When the temperature of the seaming iron was below ~190 °C, the PE 165 adhesive was not completely melted, resulting in a failure of the adhesive joint during the tensile test. As expected, the adhesive strength was weaker than the tensile strength of the metallized PEN membrane (Fig. 13). The adhesive fractured surface was investigated using a HSEM (Fig. 14). Both properly-melted web adhesive and poorly-melted web adhesive were found in the fracture surface. A small fragment of metallized PEN membrane was found near the properly-melted adhesive area (Fig. 14). Fig. 15 shows a high magnification image of properly-melted adhesive web. The surface of the web adhesive fiber was flat (Fig. 15), and Cr was found at the fracture surface of the web adhesive from the EDS analysis (Fig. 16). This indicated that there was good contact and adhesion between the adhesive and Cr layers of the other metallized PEN membrane (Kang et al., 2001). In comparison, the poorly-melted adhesive web showed the original round shape and unfused adhesive fibers (Fig. 17) and Cr was not found in the fracture surface of the adhesive web (Fig. 18), which indicates adhesive failure where insufficient melting occurred.

Table 6
Candidate hot-melt adhesives. Note that both manufacturers produce hot-melt adhesives with a range of melting points (Spunfab, n.d.; Bostik, n.d.).

Adhesive	Weight Loss		Melting Point	
	Weight loss at 110 °C for 30 min	Temperature at 5 wt% loss	Onset Point	Melting Peak
PA 1811	0.9 wt%	340 °C	50 °C	75 °C
PE 165	0.4 wt%	330 °C	140 °C	165 °C

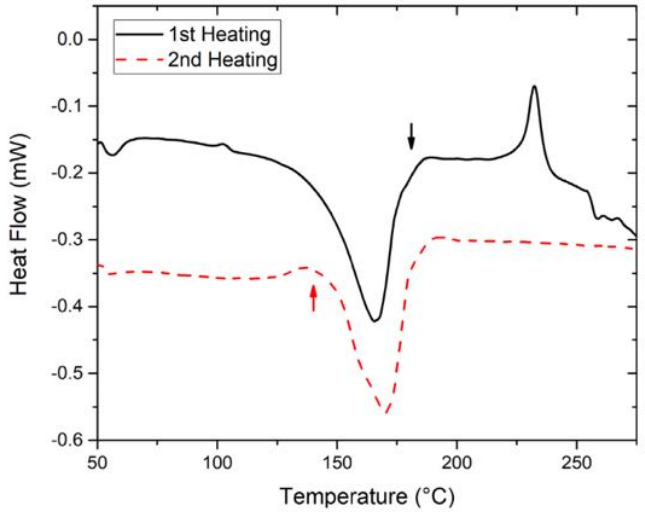

Fig. 10. MDSC thermograms of PE 165 nonwoven web adhesive.

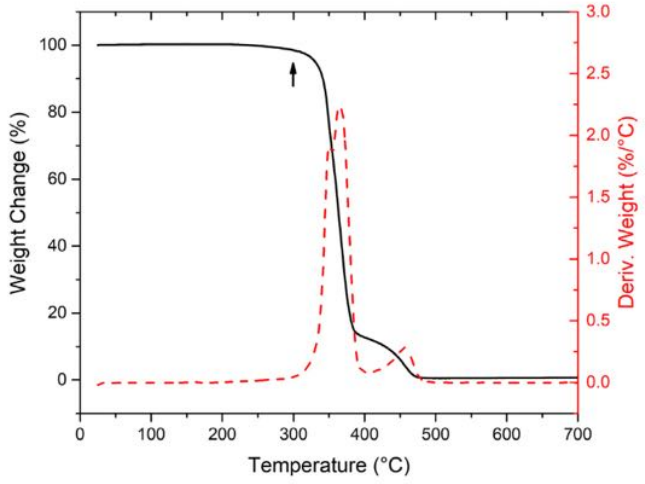

Fig. 11. TGA thermogram of PE 165 nonwoven web adhesive.

A thermostatic controlled sealing iron was used for the seaming process. The seamed joint displayed good adhesion strength while the temperature of the iron was carefully controlled to about 204 °C. Because the temperature of the iron slightly decreased below the setting temperature as it was used, the iron was allowed to heat back up for a few seconds after seaming the 0.5 m long membrane. When the test specimen failed, the metallized PEN film broke just above the adhesive area. Thus, the adhesion strength was higher than sail membrane (metallized PEN) tensile strength (Fig. 19).

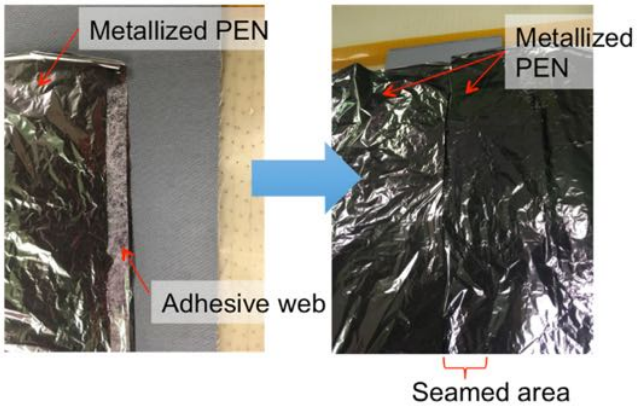

Fig. 12. Seaming process of metallized PEN gores using PE 165 nonwoven web adhesive.

From the thermal analysis of the sail membrane in orbit (Section 3.3), the expected sail temperatures range from −127 to 137 °C for the worst-case scenario during flight. The adhesion strength for this temperature range was evaluated. The temperature limits of the environmental oven chamber for the load frame was −70 to 200 °C. The quantitative adhesion test was performed in this temperature range. A qualitative cryogenic adhesion test was performed manually by immersing the sample in a dewar flask containing liquid nitrogen (−196 °C) and pulling it apart to see where the break occurred. All the specimens showed good adhesion as the membrane failed without delamination of the adhesive joint at cyrogenic temperatures.

The quantitative tensile load of the seamed joint as a function of tensile extension at different test temperatures (−70, −40, ~20, 120, 140, 160, 180, and 200 °C) were recorded until the failure of the specimens (Fig. 20). From −70 to 160 °C, all of the metallized PEN membranes broke before the adhesive joint failure, indicating cohesive failure of the membrane occurred. In general, acceptable adhesion was confirmed below 160 °C. Above 180 °C, slippage and failure of the adhesive joint occurred before cohesive failure of the membrane material due to complete melting of the PE 165 adhesive. PEN has a glass transition temperature of ~124 °C, but the high crystallinity of PEN (~54%) and metal layers (Al and Cr) help to maintain its mechanical integrity above 180 °C (Kang et al., 2017). The load at failure of the seamed joint specimens and the failure strength normalized by the sail membrane cross-section as a function of test temperature are shown in Fig. 21. Because the adhesive strength is stronger than

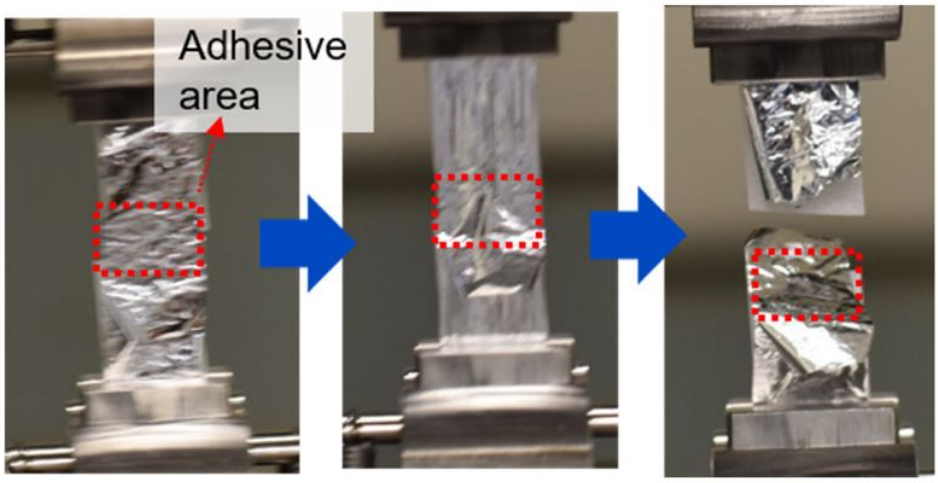

Fig. 13. An example of adhesive failure of the lap shear test specimen. The partial failure of the adhesive joint indicates generally poor or inhomogeneous adhesion.

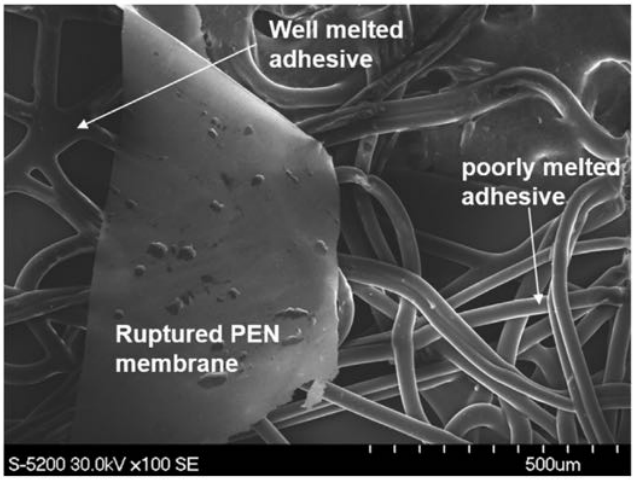

Fig. 14. HSEM image of the fracture surface of adhesive joint. Inhomogeneous melting was discovered.

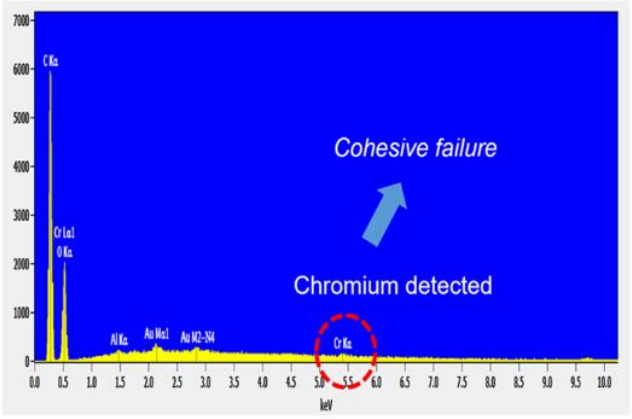

Fig. 16. EDS analysis of the fracture surface of properly-melted PE 165 adhesive.

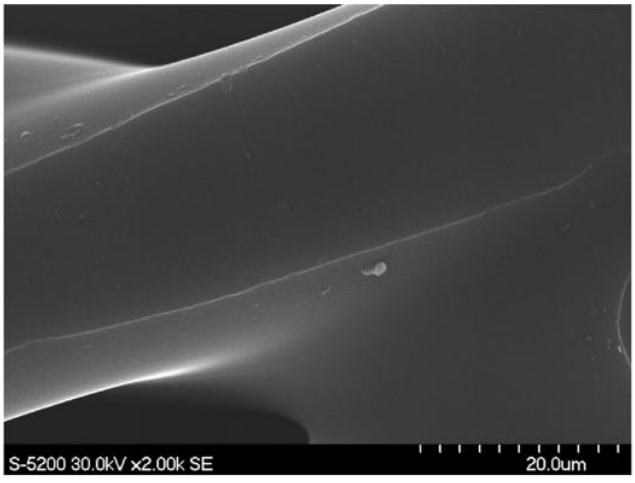

Fig. 15. HSEM image of the properly-melted PE 165 adhesive from the adhesive joint. The melted web adhesive fibers are fused and connected in a network.

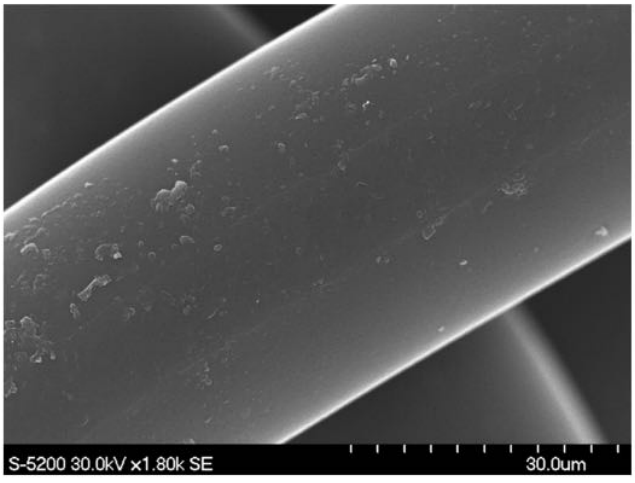

Fig. 17. HSEM image of the poorly-melted PE 165 adhesive web from the adhesive joint. The web adhesive fiber did not completely melt and fuse with other adhesive fibers.

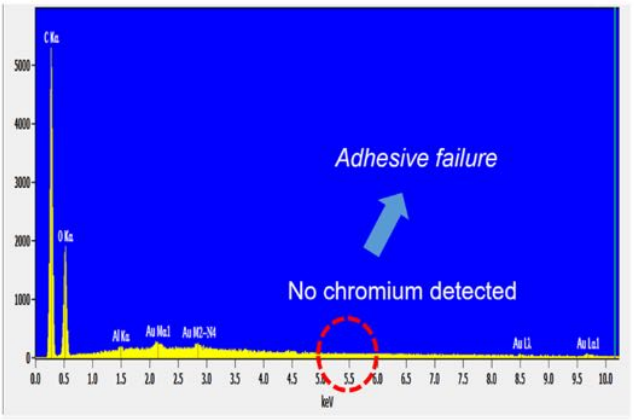

Fig. 18. EDS analysis of the fracture surface of poorly-melted PE 165 adhesive.

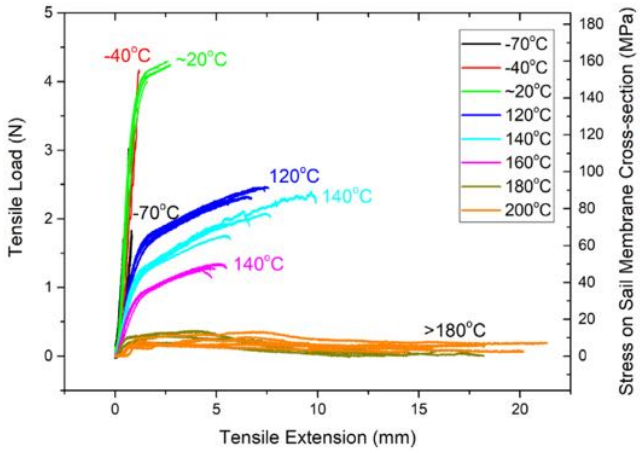

Fig. 20. Adhesion test of the seamed metallized PEN joint at temperatures from −70 to 200 °C.

the tensile strength of the metallized PEN membrane, the temperature dependency of the load at failure was determined by the intrinsic tensile strength of the PEN membrane. At room temperature (~20 °C), the tensile load at failure (or failure strength normalized by sail membrane cross-section) was about 4.2 N (155 MPa). Below room temperature, the load at failure decreased with decreasing temperature because the PEN membrane became less compliant (smaller elongation at break) at lower temperatures. Above room temperature, the load at failure decreased with increasing temperature because the stiffness (or modulus) of PEN membrane decreased. Although the test strain rate was relatively lower than the actual strain rate of deployment, for all the tests, the failure strength normalized by the cross-section was higher than the estimated maximum biaxial tension level of the solar sails (~0.02 MPa). The apparent work of adhesion was calculated from the failure load (Fig. 22). However, the actual work of adhesion can be higher than the apparent value

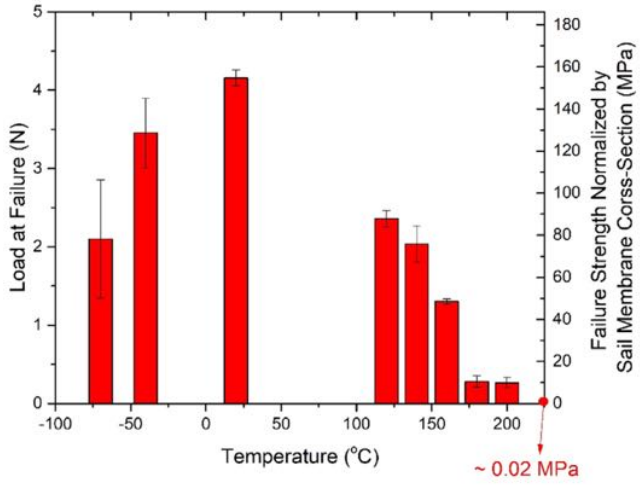

Fig. 21. Load at failure and failure strength normalized by sail membrane cross-section as a function of test temperature. Data tested at cryogenic temperature show larger deviation compared to the data tested above room temperature.

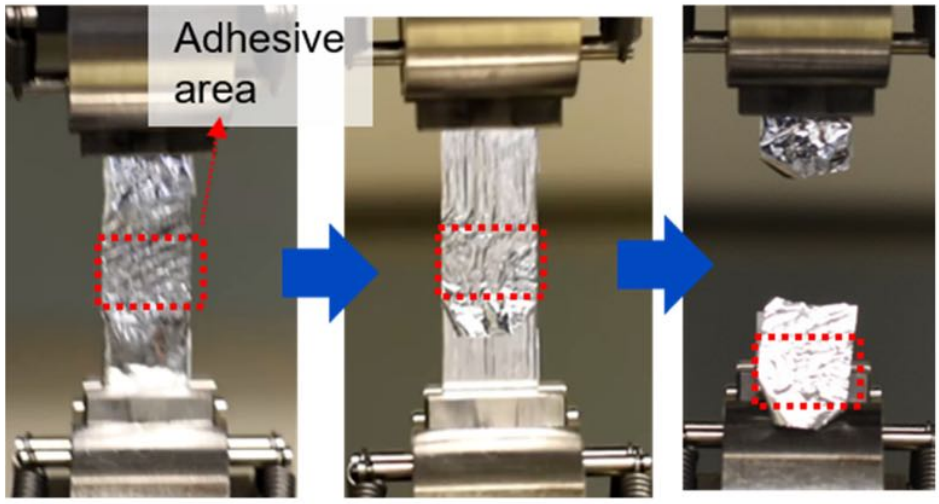

Fig. 19. An example of the adhesion test of the lap shear test specimen. The metallized PEN membrane was ruptured during the test, which indicates the adhesive joint was stronger than the tensile property of the metallized PEN membrane.

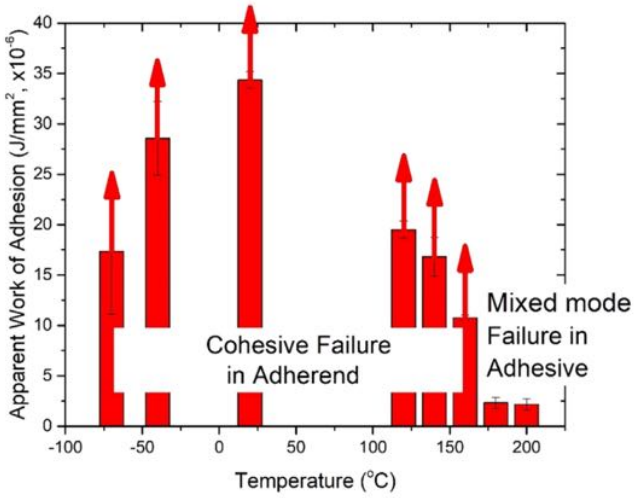

Fig 22. Apparent work of adhesion as a function of temperature. The arrows indicate that the actual work of adhesion is higher than the apparent work of adhesion because cohesive failure in adherend (sail membrane rupture) occurred. Since failure occurred in adhesive above 180 °C, the apparent work of adhesion is approximately the same as the actual work of adhesion (Kang et al., 2017).

because cohesive failure occurred (Kang et al., 2001). Since mixed mode failure occurred in the adhesive above 180 °C, the apparent work of adhesion is approximately the same as the actual work of adhesion.

Sail quadrants were successfully fabricated utilizing the optimized seaming process obtained in Section 3.6. Thirteen gores were seamed together with strips of ~10 mm wide PE 165 web adhesive [Fig. 23(a)]. Kevlar® fiber embedded adhesive joints were used as a rip stop mechanism as needed. Once all gores were seamed together, the desired quadrant planform perimeter was drawn directly onto the sail membrane and then trimmed to the final shape [Fig. 23(b)]. Next, Al grommets were added to each corner. They were sandwiched with PE 165 web adhesive and the metallized PEN, and secured by heat seaming with an iron, and perforated for tip connection to booms [Fig. 23(c and d)].

4. Summary

Optical properties of different solar sail membranes were characterized to estimate thermal equilibrium conditions of the sail membrane in space. The interface and adhesion of solar sail membrane structures were investigated. Adhesion strength between Al and PEN membrane was improved by 17% by a plasma treatment. An additional Cr tie layer between Al and the PEN membrane increased the adhesion strength by 76%. The improved metal-polymer interfacial strength can increase the stability of the Al layer during fabrication and the physical durability of seamed sail structure from folding through mission lifetime.

The adhesive quality of a commercial hot melt polyester web adhesive was investigated for seaming gores to fabricate sail quadrants. The seamed sail membranes with PE 165 web adhesive showed good adhesion strength over a temperature range of −196 °C to 160 °C, provided that optimal sealing temperatures were used. These results indicate that hot-melt adhesives are good candidate adhesives for fabricating solar sails with minimal risk of inadvertent adhesion between folds of stowed sail membranes.

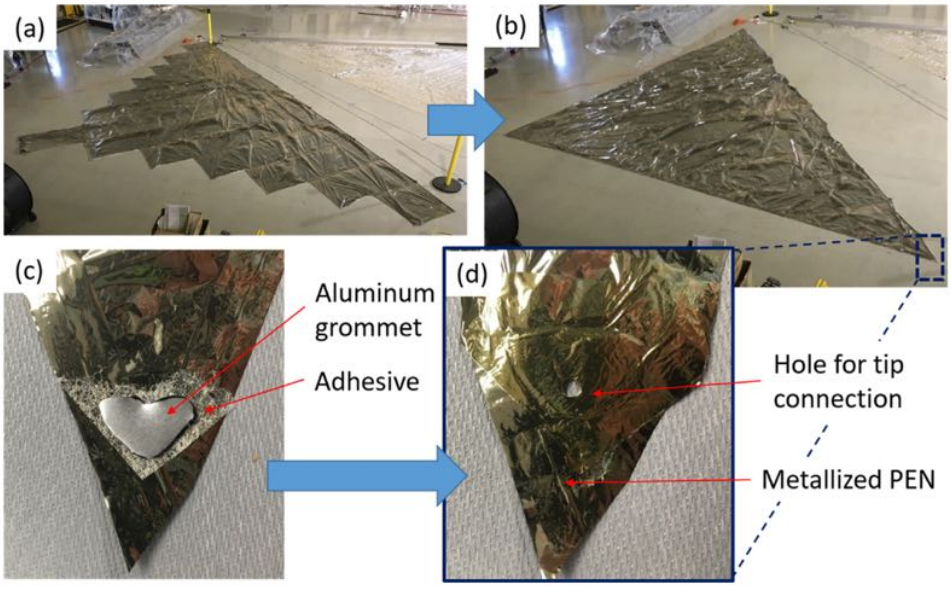

Fig. 23. A sail quadrant fabrication process. (a) seaming gores, (b) trimming, and (c–d) reinforcing vertex for durable tip connection.

Declaration of Competing Interest

The authors declare that they have no known competing financial interests or personal relationships that could have appeared to influence the work reported in this paper.

References

3M, n.d. 3M™ adhesive transfer tape 966, viewed 5 June 2019, https://3m.citrination.com/pif/000314.

Bostik, n.d. Bostik hot melt pressure sensitive adhesive, viewed 30 January 2019, https://www.bostik.com/smart-adhesives/lead-technologies/hot-melt-pressure-sensitive-adhesive/.

Cordill, M.J., Taylor, A., Schalko, J., Dehm, G., 2010. Fracture and delamination of chromium thin films on polymer substrates. Metall. Mater. Trans. A 41 (4), 870–875. https://doi.org/10.1007/s11661-009-9988-9.

Filsinger, D.H., 1995. Formaldehyde levels based on bulk and elevated temperature evolution rate measurements of silicone materials. Am. Ind. Hyg. Assoc. J. 56 (12), 1201–1207.

Gauthier, E., Pocheau, C., Kovari, M., Barnard, J.M., Crowley, B., Godwin, J., Lane, C., 2015. Thermal behaviour and temperature measurements of melting beryllium plasma-facing components exposed to high heat flux. J. Nucl. Mater. 463, 787–791.

Georgevic, R.M., 1973. The solar radiation pressure forces and torques model. J. Astronaut. Sci. 20, 251–274.

Hanrahan, F.Z., Ianno, N.J., 2014. Relationship between photofixed, effluent, and bulk composition of several room-temperature-vulcanized materials. J. Spacecr. Rock. 51 (3), 978–982.

Heiligers, J., Diedrich, B., Derbes, W., McInnes, C., 2014. Sunjammer: Preliminary end-to-end mission design. AIAA 2014-4127, AIAA/AAS Astrodynamics Specialist Conference, San Diego, CA, 4–7 August.

Kang, J.H., Cho, K., Park, C.E., 2001. Adhesion strength of poly(imide-siloxane) with Alloy 42 lead frame and silicon dioxide. Polymer 42 (6), 2513–2520.

Kang, J.H., Bryant, R.G., Wilkie, W.K., Wadsworth, H.M., Craven, P. D., Nehls, M.K., Vaughn, J.A., 2017. Simulated space environment effects on a candidate solar sail material. NASA TP 2017-219644.

Kezerashvili, R.Y., Matloff, G.L., 2007. Solar radiation and the beryllium hollow-body sail: 1. The ionization and disintegration effects. J. Br. Interplanet. Soc. 60 (5), 169–179.

Kezerashvili, R.Y., 2008. Solar sail interstellar travel: 1. Thickness of solar sail films. J. Br. Interplanet. Soc. 61 (11), 430–439.

Kezerashvili, R.Y., 2009. Thickness requirement for solar sail foils. Acta Astronaut. 65 (3-4), 507–518.

Liston, E.M., Martinu, L., Wertheimer, M.R., 1993. Plasma surface modification of polymers for improved adhesion: a critical review. J. Adhes. Sci. Technol. 7 (10), 1091–1127.

Loarer, T.h., Brygo, F., Gauthier, E., Grisolia, C., Le Guern, F., Moreau, F., Murari, A., Roche, H., Semerok, A., 2007. Surface temperature measurements by means of pulsed photothermal effects in fusion devices. J. Nucl. Mater. 363–365, 1450–1456.

MacDonald, W.A., Looney, M.K., MacKerron, D., Eveson, R., Adam, R., Hashimoto, K., Rakos, K., 2007. Latest advances in substrates for flexible electronics. J. Soc. Inf. Display 15 (12), 1075. https://doi.org/10.1889/1.2825093.

Matloff, G.L., Kezerashvili, R., 2008. Interstellar solar sailing: A figure of merit for monolayer sail. J. Br. Interplanet. Soc. 61, 330–333.

McInnes, C.R., 1999. Solar Sailing: Technology, Dynamics and Mission Applications. Springer Praxis, New York.

Petire, E.M., 2013. Adhesive bonding of textile: principles, types of adhesive and methods of use. In: Jones, G.K.S. (Ed.), Joining Textiels: Principles and Applications. Woodhead Publishing Series in Textiles, pp. 225–274.

Silvain, J.F., Ehrhardt, J.J., 1993. An overview on metal/PET adhesion. Thin Solid Films 236 (1-2), 230–235.

Spunfab, n.d. Spunfab product overview, viewed 30 January 2019, https://www.spunfab.com/product-overview/.

TSU, T.C., 1959. Interplanetary travel by solar sail. ARS J. 29 (6), 422–427.

White, C., Tan, K., Wolf, A., Carbary, L., 2010. Advances in structural silicone adhesives. In: Dillard, D.A. (Ed.), Advances in Structural Adhesive Bonding. Woodhead Publishing, pp. 66–95.

Guerrant, D.V., Lawrence, D.A., 2011. In: The Heliogyro Reloaded, Joint Army-Navy-NASA-Air Force (JANNAF) Interagency Propulsion Committee Meeting. Huntsville, AL, USA, 5–9 December.

Wilkie, W., Fernandez, J., Banicevic, P., Stohlman, O., Rose, G., Warren, J., Chamberlain, M., Kang, J., Straubel, M., Heiligers, J., 2019. An overview of NASA's advanced composite solar sail system (ACS3) low-earth orbit technology demonstration project. The Fifth International Symposium on Solar Sailing.

Xiao, H., Li, C., Yang, D., Li, X., He, S., 2008. Optical degradation of polydimethylsiloxane under 150 keV proton exposure. J. Appl. Polym. Sci. 109 (6), 4060–4064.